

**IN SITU MEASUREMENT OF FERRIC IRON IN LUNAR GLASSES USING FE-XAS: IMPLICATIONS FOR LUNAR ERUPTION MECHANISMS.** M. C. McCanta<sup>1</sup>, M. D. Dyar<sup>2</sup>, M. J. Rutherford<sup>3</sup>, A. Lanzirotti<sup>4</sup>, and S. Sutton<sup>4</sup>. <sup>1</sup>Dept. of Earth & Ocean Sciences, Tufts University, Lane Hall, Medford MA 02155 (mol-ly.mccanta@tufts.edu), <sup>2</sup>Dept. of Astronomy, Mt. Holyoke College, South Hadley MA 01075, <sup>3</sup>Dept. of Earth, Environmental, and Planetary Sciences, Brown University, Providence RI 02912, <sup>4</sup>Center for Advanced Radiation Sources (CARS), The University of Chicago, Chicago, IL 60637, USA.

**Introduction:** Oxygen is the most abundant element in solids of the solar system, and is surprisingly variable. Because oxygen is difficult to measure quantitatively through direct methods, it can best be evaluated through analysis of multivalent elements, which record oxygen potential and are quantified using the parameter of oxygen fugacity ( $f_{O_2}$ ). The prevailing  $f_{O_2}$  of an igneous system constrains phase equilibria and affects both the crystallization processes of melts and the composition of the resulting phases. Additionally,  $f_{O_2}$  also exerts control on the partitioning of elements between the core and silicate portions of terrestrial planets during planetary differentiation and plays a role in fluid-driven metasomatism, with potential linkage to atmospheric evolution.

Many existing geoanalytical techniques have been developed to identify minerals and quantify major, minor, and trace elements and isotopes at nanoscales with precision and accuracy. However, interpretable measurements of redox states at sub-nm and pm scales, particularly of glasses, have presented formidable analytical challenges. Current glass  $Fe^{3+}$  quantification methods include wet chemistry and Mössbauer, techniques that require large sample sizes and are performed on bulk material. Synchrotron X-ray absorption spectroscopy (XAS) presents the opportunity to measure  $Fe^{3+}$  at microscales *in situ*, thereby allowing for resolution of potential variations within the sample. We have developed glass calibration standards to allow for accurate XAS measurements of glasses [1,2]. We present here analyses of lunar glass  $Fe^{3+}$  contents from both Apollo 15 green glass (A15427) and Apollo 17 orange glass (A74220) samples. The presence of measureable  $Fe^{3+}$  has important implications for interpreting mechanisms of lunar glass bead eruption as well as for our understanding of the lunar interior.

#### Analytical Methods:

**Glass standardization.** A series of 33 geologically-relevant glasses (basalt-rhyolite) was synthesized over a range of  $f_{O_2}$  values (IW-air) to be used as XAS standards [2]. Fe-XAS analyses were performed on the quenched glasses at Brookhaven National Lab (BNL), beamline X26A. Mössbauer analyses of the same glasses were acquired in the Mineral Spectroscopy Lab at Mount Holyoke College to determine “true”  $Fe^{3+}$  contents. Multiple methods of data pre-processing and multivariate techniques were tested to optimize XAS

$Fe^{3+}$  measurements. Multivariate prediction models were built from Mössbauer and XAS results using the open-source machine learning Python library Scikit-learn [3], which was used to train and test partial least squares (projection to latent structures), Lasso (least absolute shrinkage and selection operator), and SVR (support vector regression) models (see [1] for a more detailed explanation). Our results show that the lasso provides significantly better results than PLS for this task.  $Fe^{3+}$  concentrations determined using Mössbauer result in an accuracy of  $\pm 1-3\%$ ; those using XAS have an accuracy rate of  $\pm 3\%$  [1,2].

**Lunar glass analyses.** Lunar glass beads from Apollo 15 and Apollo 17 were also studied at BNL beamline X26A under the same conditions as those of the standards (beam size  $\sim 2-5 \mu m$ ). Major element compositions of the same locations were analyzed on the Cameca SX-100 at Brown University. Glass analyses were obtained using a 15 kV acceleration voltage, 10 nA beam current, and a defocused 5-15  $\mu m$  beam.  $Fe^{3+}$  contents of lunar glasses were determined using the lasso model trained on the calibration standards.

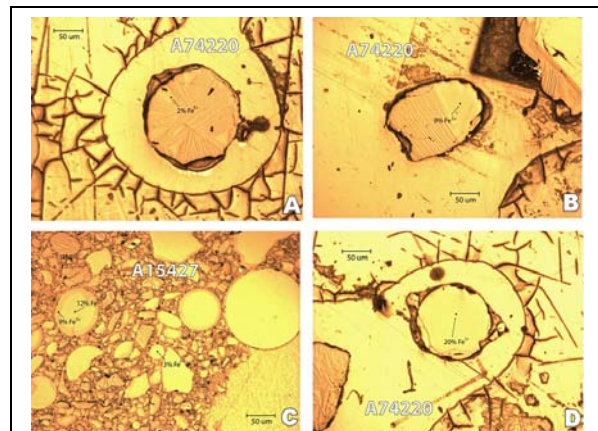


**Figure 1.** Reflected light photomicrographs of analyzed glass beads.  $Fe^{3+}$  contents are indicated on the image.

**Results:** Ferric iron was observed in all of the lunar glasses analyzed (Fig. 1).  $Fe^{3+}$  contents ranged from 2-20%. No differences in  $Fe^{3+}$  contents were observed between the orange and green glasses in the 20 beads analyzed.  $Fe^{3+}$  was low in partially crystalline glass beads (Figs. 1A,B) and in smaller holohyaline beads (Fig. 1C). The highest measured  $Fe^{3+}$  was in a large, holohyaline bead in A74220 (Fig. 1D). In addition, the core and rim of several zoned glass beads

were analyzed in A15427.  $\text{Fe}^{3+}$  appears to be zoned from high core to lower rim, although the difference is near the limit of analytical accuracy (Fig. 1C).

**Discussion:** Reports of  $\text{Fe}^{3+}$  in lunar materials, both glasses [4] and minerals [5,6], go back decades. The lunar interior  $f_{\text{O}_2}$  however, is  $\sim$ IW-1 [7,8], a region where significant  $\text{Fe}^{3+}$  is not expected to be present. However, recent studies indicate the Moon is not as dry as previously thought [i.e., 9,10]. The presence of  $\text{Fe}^{3+}$  in lunar glasses may well be related to the oxidizing potential of the newly recognized lunar  $\text{H}_2\text{O}$ .

The range of  $\text{Fe}^{3+}$  contents observed in the glasses may result from degassing processes during magma ascent. Previous theories on lunar fire fountain eruptions suggested that graphite in the melt scavenged oxygen from metal oxides to produce CO gas [11-13] during ascent from the lunar interior. This occurred as decreasing pressure stabilized CO over graphite. Production of CO gas therefore resulted in the reduction of metal oxides. Reduced FeNiCo-metal beads have been observed in many lunar glass beads [e.g., 14].

It is still possible that some graphitic C was carried by the ascending picritic magmas; however, recent experiments show that this is not necessary [15]. With 100's to 1000 ppm H present, Wetzel et al. [15] find that CO is dissolved as Fe-carbonyl in a C-saturated picritic melt at IW-1.0 and pressures up to 1000 MPa. Because C and H decrease with decreasing P, the first lunar gas phase would have been formed as Fe-carbonyl saturation was exceeded in a rising magma. Analyses of melt inclusions in orange glass olivine crystals show decreases in C and S with H trending toward the low contents in the associated glass beads [16], confirming this conclusion. It appears an orange glass magma would produce a CO-rich gas phase deep in the lunar crust [17]. This gas phase may have originated even deeper based on the volume of the gas bubbles found in several of the melt inclusions [16].

Breakdown of Fe-carbonyl during magma ascent could also explain formation of Fe-metal beads in picritic glasses [14]. Magma degassing at depth might have been close to an equilibrium process, despite the presence of FeNiCo metal beads. Beads trapped in orange glass olivine crystals are homogeneous  $\text{Fe}_{85}\text{Ni}_{14}\text{Co}_1$  [14], but those in glass show strong zoning to Ni-rich rims [14], indicating an oxidation event late in the ascent process. Perhaps this degassing oxidized the remaining melt (and metal) as volatile cations coordinated with O in the melt entered the gas, leaving excess O in the melt [14]. Kinetic degassing of glass beads after near-surface fragmentation (bead-formation) is indicated by different diffusion-loss profiles [9]. If H was lost by H diffusion from an OH or  $\text{H}_2\text{O}$  dissolved species, oxidation would result.

Later oxidation observed in high-Ni rims of metal beads in the glasses may also be responsible for  $\text{Fe}^{3+}$  contents observed in this study. The lowest  $\text{Fe}^{3+}$  contents are recorded in smaller diameter beads (Fig. 1C) or near bead rims (Figs. 1A-C), while the highest  $\text{Fe}^{3+}$  concentration (20%) was measured in the center of a large, holohyaline glass bead (Fig. 1D). If H loss is causing oxidation, then the smaller beads and bead rims, which would be quenched more quickly than the larger beads or bead interiors, may not be subjected to significant oxidation. The larger, more slowly cooled beads would experience greater time for oxidation to take place, therefore higher  $\text{Fe}^{3+}$ .

The low  $\text{Fe}^{3+}$  observed in the partially crystalline beads (Figs. 1A-B) may be the result of analytical location. Although these beads cooled more slowly than the holohyaline samples, the olivines in these beads are dendritic indicating they are of the most rapidly cooled crystalline variety [18]. Due to their slower cooling rate, higher  $\text{Fe}^{3+}$  might be expected. However, in both of the beads studied, XAS analyses were made near the rim, a region likely to have experienced more rapid cooling and therefore less oxidation. Further analyses (i.e., traverses) of different regions in partially crystalline beads are required to better constrain this process.

**Future Work:** To more fully document the range of  $\text{Fe}^{3+}$  contents present in lunar glasses, additional XAS measurements are planned for an expanded suite of samples. These include glasses from all Apollo missions, including volcanic glass beads and magmatic and agglutanic glasses. In addition, XAS traverses are planned to study potential  $\text{Fe}^{3+}$  zonation.

**Acknowledgments:** Research supported by NSF grants EAR-1219761 and EAR-1219850 and RIS<sup>4</sup>E, SEED, and VORTICES nodes of NASA SSERVI.

**References:** [1] McCanta M.C. et al. (this volume) *LPS XXXVI*. [2] Dyar M.D. & McCanta M.C. (2014) *AGU Fall Mtg.*, A4858. [3] Pedregosa F. et al. (2011) *J. Machine Learning Res.*, 12, 2825-2830. [4] Dyar M.D. & Consolmagno G.J. (1982) *LPS XIII*, 193-194. [5] Niebuhr H.H. et al. (1973) *LPS III*, 971-982. [6] Schürmann K. & Hafner S.S. (1972) *LPS III*, 615-621. [7] Sato M. (1976) *LPS VII*, 1323-1344. [8] Nicholis M. & Rutherford M.J. [9] Saal A.E. et al. (2008) *Nature*, 454, 192-196. [10] McCubbin F.M. et al. (2010) *Am. Mineral.*, 95, 1141-1150. [11] Sato M. (1979) *LPS X*, 311-325. [12] Fogel R.A. & Rutherford M.J. (1995) *Geochim. Cosmochim. Acta*, 59, 201-215. [13] Rutherford M.J. & Papale P. (2009) *Geology*, 37, 219-222. [14] Weitz C.M. et al. (1997) *Geochim. Cosmochim. Acta*, 61, 2765-2775. [15] Wetzel D.T. et al. (2013) *PNAS*, doi: 10.1073/pnas.1219266110. [16] Hauri E.H. et al. (2011) *Science*, 333, 213-215. [17] Wetzel D.T. et al. (2014) *LPS XXXV*. [18] Heiken G.H. & McKay D.S. (1978) *LPS IX*, 1933-1943.